IEEE Access
Multidisciplinary | Rapid Review | Open Access Journal

Received April 1, 2022, accepted April 13, 2022, date of publication April 29, 2022, date of current version May 16, 2022.

Digital Object Identifier 10.1109/ACCESS.2022.3171345

Distributed Model Predictive Voltage Control for Distribution Grid Based on Relaxation and Successive Distributed Decomposition

EDOARDO DE DIN[1], MARTINA JOSEVSKI[1], MARCO PAU[2], (Member, IEEE), FERDINANDA PONCI[1], (Senior Member, IEEE), AND ANTONELLO MONTI[1,3], (Senior Member, IEEE)

[1]Institute for Automation of Complex Power Systems, RWTH Aachen University, 52074 Aachen, Germany
[2]Department of Grid Planning and Operation, Fraunhofer Institute for Energy Economics and Energy System Technology, 34119 Kassel, Germany
[3]Fraunhofer FIT, 52062 Aachen, Germany

Corresponding author: Edoardo De Din (ededin@eonerc.rwth-aachen.de)

This work was supported by EdgeFLEX, which is a European project. This project has received funding from the European Union's Horizon 2020 research and innovation programme under grant agreement No 883710.

ABSTRACT Advanced control techniques for modern distribution grids are becoming fundamental for the reduction of grid reinforcements while maintaining network performances. In particular, as shown in literature, distributed algorithms for voltage control have gained much interests in comparison with the typical centralized formulation for its feasibility. Distributed model predictive control (MPC) is shown to optimally manage the Distributed Generators (DGs) over time and it can be implemented locally at the controllable sources. For this purpose, this paper adopts a distributed algorithm recently presented in the literature for solving a constraint-coupled optimization problem for model predictive voltage control. A detailed reformulation of the original MPC problem for the specific application is presented. Besides, this paper provides a calculation of the convergence limit for the value of the iteration step size of the algorithm, supported by numerical results. The proposed distributed solution of model predictive voltage control is compared with a centralized formulation via numerical simulation in terms of the percentage of error with the centralized solution and number of iteration for the convergence.

INDEX TERMS Voltage control, distributed optimization, smart grids, networked control systems.

I. INTRODUCTION

Due to an increasing penetration of Distributed Generators (DGs), distribution grids are turning into active distribution networks that require new solutions to satisfy the limits on the voltage defined by grid standards [1], [2]. To mitigate voltage violations occurring in the distribution grid during normal operating condition, different actions can be adopted: grid reinforcements, local control, meaning controllers that operates using local voltage measurement and do not exchange data with neighbors or a central controller (e.g. droop-based control [3], [4]), or smart control techniques. Grid reinforcements consist in the physical update of the assets installed in the network and it represents one of the possible solution adopted by the Distributions System Operators (DSOs). Distribution grid can also present some DGs installed with the capability of locally providing reactive power to compensate for voltage deviations via local control techniques, however this approach does not result in an optimal solution for the grid and it does not coordinate the resources [5]. Smart control techniques that coordinate the installed DGs to reach a system-level solution, do not represent at the moment the common approach followed by DSOs, however some new regulations are attempting to shift the focus to alternative, digitalized control techniques for distribution networks [6]. These solutions make use of the on-site communication network, monitoring system and controllable DGs to prevent overvoltage or undervoltage events by providing control set-points to the controllable assets, so as to reduce the need for grid reinforcements [7]–[9]. The control structures developed for the voltage control of distribution grids have been originally expressed in a centralized

The associate editor coordinating the review of this manuscript and approving it for publication was Yang Li.

formulation, meaning that optimal control problem is solved entirely by a single controller [10]–[12]. More recently the research has shifted towards distributed voltage control solutions in which the optimal control problem is solved separately by the agents of a network, which compute only their portion of the optimal solution and communicate with a limited number of neighboring agents [13]–[15]. In comparison with the centralized solution, each agent only shares limited amount of information with the agents located in the neighbourhood, improving therefore security [15]. Distributed algorithms are also more robust with respect to sudden disconnection of individual agents or to reconfiguration of the grid [16].

A possible voltage control strategy that can be applied in both centralized and distributed architecture is the Model Predictive Control (MPC), where the optimization problem is solved by minimizing the objective function over a finite prediction horizon. As described in [17], since the MPC performs an optimization using measurements and predictions, it is able to track reference values provided with larger timescale while correcting voltage deviations with online measurements. Purpose of the MPC described in this paper is to track the reference value for the State of Charge (SoC) over a finite time horizon while maintaining the voltage in the operational limits. To track the reference, the dynamic of the State of Charge (SoC) of the Energy Storage Systems (ESSs) is thus included in the control formulation.

The proposed distribution of the MPC for voltage control problems is based on a cooperative scheme, where the local controller of each autonomous agent collaborates with the other controllers in a network to achieve a global objective [18], [19]. Moreover, the proposed approach relies on the fact that some optimization problems can be formulated as a constraint-coupled set-up, meaning that the global cost function is defined as the sum of local functions, where each single variable only depends on local constraints with additional global coupling constraints to be met [20], [21]. In [20] the authors present a distributed solution for constraint-coupled set-up without a central update step involving communication among all the agent. However this solution requires the exchange of the result of the local dual optimization among the agents. This requirement is removed in [21] where a distributed solution based on dual decomposition and proximal minimization has been presented. With this approach only the dual variables are exchanged among the neighbors, enhancing the security, but an averaging mechanism is required to recover primal optimality (Step 7 of the algorithm). An innovative solution to solve constraint-coupled optimization problem in a distributed manner is introduced in [22], in which the relaxation on the local variables is combined with the successive duality to achieve a distributed optimization algorithm. The algorithm, named by the authors Relaxation and Successive Distributed Decomposition (RSDD), has the advantage that primal optimization solution is obtained without averaging, thus increasing convergence speed, it does not require particular initialization and the local variables are not exchanged. Moreover this approach adds a relaxation to the original problem, allowing local violations of the constraints without assuming *a priori* feasibility of the local problem.

The Distributed MPC formulated in this paper is meant to operate online [23]–[25], which in comparison with the offline solution, the calculation of the control output and the transmission of the set-points to the controllable devices need to be performed in fixed time steps. This means that it requires fairly fast algorithm with possibly the ability to obtain a high convergence speed. Based on these requirements the RSDD has been chosen for the implementation of the proposed Distributed MPC for voltage control, given that, as proposed in [22], it features local computation of only local variables with no averaging mechanism, the possibility of having a scaled relaxation and the absence of initialization requirement

This paper presents the application of the RSDD to the model predictive voltage control problem. Firstly the model predictive voltage control problem is reformulated into a constraint-coupled set-up to apply the algorithm, then the algorithm is applied to the new formulation by following the approach presented in [22]. Moreover this paper provides, based on the graph configuration and on the constraint functions of the optimization problem, a calculation for the limit value of the coefficient that control the step length of the algorithm.

The rest of the paper is structured as follows: Section II formalizes the voltage control problem and describes the general MPC problem for voltage control. Section III briefly introduce the theory behind the RSDD algorithm. Section IV describes the general MPC problem for voltage control and the application of the RSDD to it. Section V presents the calculation of the convergence limit for the parameter that control the stepsize of the algorithm. Section VI presents the simulation setup used for the tests and shows the results obtained in different simulation scenarios. Finally, Section VII summarizes the main highlights of this work and concludes the paper.

II. VOLTAGE CONTROL PROBLEM FORMULATION

A. PROBLEM DESCRIPTION

Based on the linearized branch-flow model for radial distribution networks [26], the voltage phasors of the nodes can be expressed in terms of real and imaginary current injections. However, using per unit quantities and neglecting the high order real and reactive power loss terms, the current phasors can be replaced with the corresponding real and imaginary components of the complex power. Moreover, since distribution grids are usually operated with large power factors, the real component of the voltage phasor can be approximated with its magnitude and the imaginary part can be neglected [27]. Therefore the vector of the bus

voltage magnitudes with the above approximation can be described as:

$$\mathbf{V} = \mathbf{1}V_0 + \mathbf{R}(\mathbf{p}^g - \mathbf{p}^c) + \mathbf{X}(\mathbf{q}^g - \mathbf{q}^c) \tag{1}$$

where:

- $\mathbf{V}$ is the vector of the voltage magnitudes
- $\mathbf{1}V_0$ is the vector of voltage magnitude of the slack bus
- $\mathbf{R}$ and $\mathbf{X}$ are the real and imaginary part of the impedance matrix of the grid.
- $\mathbf{p}^g$ and $\mathbf{q}^g$ are the vectors of the generated active and reactive power, whereas $\mathbf{p}^c$ and $\mathbf{q}^c$ are the vectors of the absorbed active and reactive power.

Equation (1) shows that a positive unbalance between generation and load causes an increase of the voltage along the feeders of the grid, whereas a negative unbalance produces the opposite effect. Therefore voltage can be decreased along the nodes by reducing the amount of generated active power or by absorbing reactive power. Conversely, the increase of the voltage can be obtained by an increment of the generated active power or by generating positive reactive power.

As shown in equation (8) of [28], defining $\mathbf{V}^n$ as the voltage that the system would have without the application of any control on the active power curtailment ($\mathbf{P}_{DG}^{curt}$) and the reactive power ($\mathbf{Q}_{DG}$) of the DGs and without the application of any control on the active power of the ESSs ($\mathbf{P}_{ESS}$), the voltage $\mathbf{V}$ is obtained by superimposing the effects of the different power injections to the uncontrolled voltage value $\mathbf{V}^n$ as follow:

$$\mathbf{V} = \mathbf{V}^n + \mathbf{R}\mathbf{P}_{DG}^{curt} + \mathbf{X}\mathbf{Q}_{DG} + \mathbf{R}\mathbf{P}_{ESS} \tag{2}$$

Purpose of the MPC for voltage control is to optimize the use of $\mathbf{P}_{DG}^{curt}$, $\mathbf{Q}_{DG}$ and $\mathbf{P}_{ESS}$ to maintain the voltage between the operational limits over a predicted horizon, while eventually tracking some reference values.

B. CENTRALIZED MPC FORMULATION

The definition of the centralized MPC formulation presented in this section is used to derive the distributed formulation in the following sections. Moreover the results obtained by solving the centralized MPC will be use to validate the results of the distributed MPC. The MPC formulation used in our work is based on [17], where the MPC problem has been formulated for a radial distribution grid described using the linearized branch-flow equations defined in [15], [26], [28], with voltage phase angles considered equal to zero. When applying MPC, at every time step k we solve a finite-time optimal control problem over a prediction horizon of $N_p = [k+1 \mid k, \ldots, k+N_p \mid k]$ time steps. After the optimization only the first step of the control output calculated for the whole prediction horizon is applied to the system and the optimization is executed again over a shifted horizon at time $k+1$. In the remainder, the expression $x_{k+s|k}$ (where x is a generic variable of the optimization problem) refers to the prediction of the variable at the future time step $k+s$ given information at the time k, with s the internal index of the prediction.

In a centralized formulation the objective function of the MPC is to minimize the quadratic expression of the difference between the optimization variables and their reference values, as follows:

$$\begin{aligned}\sum_{s=1}^{\mathbf{N}_p} &(\mathbf{P}_{DG,k+s|k}^{curt} - \mathbf{P}_{DG,k+s}^{ref})^T \mathbf{W}_P (\mathbf{P}_{DG,k+s|k}^{curt} - \mathbf{P}_{DG,k+s}^{ref}) \\ &+ (\mathbf{Q}_{DG,k+s|k} - \mathbf{Q}_{DG,k+s}^{ref})^T \mathbf{W}_Q (\mathbf{Q}_{DG,k+s|k} - \mathbf{Q}_{DG,k+s}^{ref}) \\ &+ (\mathbf{SoC}_{k+s|k} - \mathbf{SoC}_{k+s}^{ref})^T \mathbf{W}_{SoC} (\mathbf{SoC}_{k+s|k} - \mathbf{SoC}_{k+s}^{ref})\end{aligned} \tag{3}$$

where:

- $\mathbf{SoC}_{k+s|k} \in \mathbb{R}^{N_{tot}}$ is the vector of SoC values of all available storage units, with N_{tot} the total number of the grid nodes,
- $\mathbf{P}_{DG,k+s|k}^{curt} \in \mathbb{R}^{N_{tot}}$ is the vector of active power curtailments of DG units,
- $\mathbf{Q}_{DG,k+s|k} \in \mathbb{R}^{N_{tot}}$ is the vector of reactive power set-points assigned to the DGs,
- $\mathbf{P}_{DG,k+s}^{ref} \in \mathbb{R}^{N_{tot}}$, $\mathbf{Q}_{DG,k+s}^{ref} \in \mathbb{R}^{N_{tot}}$, $\mathbf{SoC}_{k+s}^{ref} \in \mathbb{R}^{N_{tot}}$ are the corresponding reference values while,
- $\mathbf{W}_P \in \mathbb{R}^{N_{tot} \times N_{tot}}$, $\mathbf{W}_Q \in \mathbb{R}^{N_{tot} \times N_{tot}}$, $\mathbf{W}_{SoC} \in \mathbb{R}^{N_{tot} \times N_{tot}}$ are the positive definite weighting matrices.

Adding the constraints, the MPC problem for the objective function (3) is defined as follows:

$$\underset{\mathbf{P}_{DG,\cdot|k}^{curt}, \mathbf{Q}_{DG,\cdot|k}, \mathbf{P}_{ESS,\cdot|k}}{\text{minimize}} \quad \mathbf{C}(\mathbf{P}_{DG,\cdot|k}^{curt}, \mathbf{Q}_{DG,\cdot|k}, \mathbf{P}_{ESS,\cdot|k}) \tag{4}$$

$$\begin{aligned}\text{subject to } a)\ & \mathbf{1}V_{min} \le \mathbf{V}_{k+s|k} \le \mathbf{1}V_{max}, \\ b)\ & \mathbf{V}_{k+s} = \mathbf{V}_{k+s-1} \\ & + \mathbf{R}(\mathbf{P}_{DG,k+s-1}^{curt} + \mathbf{P}_{ESS,k+s-1}) \\ & + \mathbf{X}(\mathbf{Q}_{DG,k+s-1}) \\ c)\ & -\mathbf{P}_{DG,k+s}^{max} \le \mathbf{P}_{DG,k+s|k}^{curt} \le 0, \\ d)\ & \mathbf{Q}_{DG,k+s}^{min} \le \mathbf{Q}_{DG,k+s|k} \le \mathbf{Q}_{DG,k+s}^{max}, \\ e)\ & \mathbf{P}_{ESS,k+s}^{min} \le \mathbf{P}_{ESS,k+s|k} \le \mathbf{P}_{ESS,k+s}^{max}, \\ f)\ & \mathbf{SoC}_{k+s} = \mathbf{SoC}_{k+s-1} - \frac{\mathbf{P}_{ESS,k+s-1}}{\mathbf{C}_{ESS}} \eta_{ESS} \\ g)\ & \mathbf{SoC}^{min} \le \mathbf{SoC}_{k+s|k} \le \mathbf{SoC}^{max},\end{aligned} \tag{5}$$

where:

- $\mathbf{1}V_{min}$, $\mathbf{1}V_{max}$ are the vectors of the minimum and maximum limits for the voltage values.
- $\mathbf{P}_{DG,k+s}^{max}$ is the vector of maximum available active power of the DGs at prediction timestep $k+s$
- $\mathbf{Q}_{DG,k+s}^{min}$, $\mathbf{Q}_{DG,k+s}^{max}$ are the vectors of minimum and maximum available reactive power of the DGs at prediction timestep $k+s$
- $\mathbf{P}_{ESS,k+s}^{min}$, $\mathbf{P}_{ESS,k+s}^{max}$ are the vectors of minimum and maximum constraints for power injection of the ESSs at prediction timestep $k+s$.
- $\mathbf{SoC}^{min}$, $\mathbf{SoC}^{max}$ are the vectors of minimum and maximum constraints SoC for the ESSs, which should be implemented as soft constraints.

- $\mathbf{C}_{ESS}$ and η_{ESS} are coefficients representing the capacity and the efficiency of the ESSs.
- $\mathbf{V}_{k+s}$ is the vector of voltage magnitudes calculated at timestep $k+s$ of the prediction horizon as function of the vector of voltage magnitudes calculated at previous timestep and of the active power of the DGs and ESSs and of the reactive power of the DGs.

When the MPC problem (3) is applied online, the values $\mathbf{P}^{curt}_{DG,k+s-1}$, $\mathbf{Q}_{DG,k+s-1}$, $\mathbf{P}_{ESS,k+s-1}$, $\mathbf{SoC}_{k+s-1}$ and $\mathbf{V}_{k+s-1}$ with $s = 0$ represents the measurements that are collected from the sensors and DGs installed in the field, whereas the values for $s \neq 0$ are obtained from the previous time step of the predicition horizon. To simplify the notation, in the rest of the paper the term $k+s \mid k$ is substituted with $\cdot \mid k$.

III. RELAXATION AND SUCCESSIVE DISTRIBUTED DECOMPOSITION

As extensively described in [22], the RSDD algorithm is based on the relaxation and on the consecutive application of two duality steps employed on a constraint-coupled optimization setup. The relaxation avoids the need to ensure *a priori* the feasibility of local problems by allowing (scalar) violations of local constraints and permitting the algorithm to be distributed. The successive application of the duality principle allows the application of the dual decomposition to the relaxed optimization problem, while then subgradient method is used to solve it.

In the general formulation, the RSDD is applied to a constraint-coupled optimization problem with separable cost function as follows:

$$\begin{aligned} &\underset{\mathbf{x}_1,\ldots,\mathbf{x}_N}{\text{minimize}} \sum_{i=1}^{N} f_i(\mathbf{x}_i) \\ &\text{subject to} \quad \mathbf{x}_i \in \mathbf{X}_i, \quad i \in 1,\ldots,N \\ &\qquad \sum_{i=1}^{N} \mathbf{g}_i(\mathbf{x}_i) \leq \mathbf{0} \end{aligned} \tag{6}$$

where, for all $i \in \{1,\ldots,N\}$, the set $\mathbf{X}_i \subseteq \mathbb{R}^{n_i}$ is a nonempty compact convex set with $n_i \in \mathbb{N}$, the convex functions $f_i(\mathbf{x}_i) : \mathbb{R}^{n_i} \to \mathbb{R}$ and $\mathbf{g}_i(\mathbf{x}_i) : \mathbb{R}^{n_i} \to \mathbb{R}^S$ with $S \in \mathbb{N}$.

Considering that a *connected* and *undirected* graph $\mathcal{G} = (\{1,\ldots,N\}, \mathcal{E})$ with $\mathcal{E} \subseteq \{1,\ldots,N\} \times \{1,\ldots,N\}$ the set of edges of the graph exists, the resulting RSDD algorithm applied to (6) is based on the following steps:

1) calculation of $((\mathbf{x}_i(t+1), \rho_i(t+1), \boldsymbol{\mu}_i(t+1))$ as solution of:

$$\begin{aligned} &\underset{\mathbf{x}_i,\rho_i}{\text{minimize}}\, f_i(\mathbf{x}_i) + M\rho_i \\ &\text{subject to} \quad \rho_i \geq 0, \quad \mathbf{x}_i \in \mathbf{X}_i \\ &\qquad \mathbf{g}_i(\mathbf{x}_i) + \sum_{j\in P_i} (\boldsymbol{\lambda}^{ij}(t) - \boldsymbol{\lambda}^{ji}(t)) \leq \rho_i \mathbf{1} \end{aligned} \tag{7}$$

2) update of the neighboring variables $\boldsymbol{\lambda}^{ij}$ for all $j \in P_i$:

$$\boldsymbol{\lambda}^{ij}(t+1) = \boldsymbol{\lambda}^{ij}(t) + \gamma(\boldsymbol{\mu}^i(t+1) - \boldsymbol{\mu}^j(t+1)) \tag{8}$$

where $\boldsymbol{\mu}^i \in \mathbb{R}^S$ is the vector of multipliers linked to the inequality constraints in (7) and obtained by the solution of the local problem (7), whereas neighboring variables $\boldsymbol{\lambda}^{ij} \in \mathbb{R}^S, j \in P_i$ are lagrangian multipliers associated with the node i and its set of neighbors P_i. The updated values of $\boldsymbol{\lambda}^{ij}$ are exchanged at each iteration of the algorithm among the neighbors, which are defined by the configuration of the graph. The variables $\boldsymbol{\lambda}^{ij}$ can also be grouped in a vector $\boldsymbol{\Lambda} \in \mathbb{R}^{(S\times|\mathcal{E}|)}$, with $|\mathcal{E}|$ being the number of elements of $\mathcal{E}$. The coefficient γ represents the step-size of the iterative calculation of $\boldsymbol{\lambda}^{ij}(t+1)$, which consequently control the convergence speed of the algorithm with t the iteration time of the algorithm. Its value, however cannot be arbitrarily selected given that a too large value of γ could lead to the non-convergence of the algorithm. Therefore in Section V, a method to calculate the converge limit of γ is presented. The variable ρ_i allows the violation $\rho_i\mathbf{1}$ of the local constraints and it is minimized in the local cost function scaled by a factor M. The value of M, whose impact has been analyzed (also numerically) in [29], has to satisfy the condition of Theorem II.6 defined in [22], meaning that $M > \|\boldsymbol{\mu}^*\|_1$ with $\boldsymbol{\mu}^*$ being an optimal solution of the dual of problem (6). The RSDD has been demonstrated to converge to an optimal cost with the limit point $\bar{\mathbf{x}} = (\bar{\mathbf{x}}_1,\ldots,\bar{\mathbf{x}}_N)$, with $\bar{\mathbf{x}}$ being a feasible solution for the original problem (6). In this paper the RSDD is iterated for a fixed number of iterations $t = t_{FIN}$ defined *a priori*.

IV. APPLICATION OF THE RSDD TO THE MPC MODEL

A. OBTAIN A CONSTRAINT-COUPLED SETUP

To obtain a constraint-coupled set-up, the MPC problem (4) has to be reformulated as function of the only variables $\mathbf{P}^{curt}_{DG,k}$, $\mathbf{Q}_{DG,k}$, $\mathbf{P}_{ESS,k}$. Moreover the problem must be reshaped in order to consider only the nodes of the grids that are part of the graph $\mathcal{G}$. In the proposed approach we consider that DGs and ESSs are both installed in each node $i \in N$, where N can be less or equal to the total number of the grid nodes N_{tot}.

Using the constraint (f) of (4), the objective function (3) can be separated into three different contribution as follows.

$$\begin{aligned} &\triangleright\ \mathbf{y}^T_{P,DG,\cdot|k} \mathbf{W}_P \mathbf{y}_{P,DG,\cdot|k} \\ &\triangleright\ \mathbf{y}^T_{Q,DG,\cdot|k} \mathbf{W}_Q \mathbf{y}_{Q,DG,\cdot|k} \\ &\triangleright\ \mathbf{y}^T_{P,ESS,\cdot|k} H^2 \mathbf{W}_{SoC} \mathbf{y}_{P,ESS,\cdot|k} \\ &+2 \cdot \mathbf{e}^T_{SoC,k-1} \mathbf{W}_{SoC} \mathbf{y}_{P,ESS,\cdot|k} \end{aligned} \tag{9}$$

where the resulting new variables are described in the Appendix A.

Considering the equation (2), the matrixes $\mathbf{R}_{DG}$, $\mathbf{X}_{DG}$ and $\mathbf{R}_{ESS}$ can be obtained by resizing the full matrixes $\mathbf{R}$ and $\mathbf{X}$ taking into account only the nodes N where DGs and ESSs are installed. The same resizing procedure is applied to the vectors $\mathbf{P}^{curt}_{DG,\cdot|k}$, $\mathbf{Q}_{DG,\cdot|k}$ and $\mathbf{P}_{ESS,\cdot|k}$ and the voltage vectors $\mathbf{V}_{\cdot|k}$ and $\mathbf{V}^n_{\cdot|k}$ are also resized accordingly. Consequently, substituting the resized voltage expression (2), the constraints of (4) can be reformulated as follows:

— Coupling constraints:

$$a.1)\begin{cases}\mathbf{R}_{DG}\mathbf{y}_{P,DG,\cdot|k} \leq \mathbf{1}V_{max} - \mathbf{V}^{n}_{\cdot|k}\\ \mathbf{1}V_{min} - \mathbf{V}^{n}_{\cdot|k} \leq \mathbf{R}_{DG}\mathbf{y}_{P,DG,\cdot|k}\end{cases}$$
$$a.2)\begin{cases}\mathbf{X}_{DG}\mathbf{y}_{Q,DG\cdot|k} \leq \mathbf{1}V_{max} - \mathbf{V}^{n}_{\cdot|k}\\ \mathbf{1}V_{min} - \mathbf{V}^{n}_{\cdot|k} \leq \mathbf{X}_{DG}\mathbf{y}_{Q,DG,\cdot|k}\end{cases}$$
$$a.3)\begin{cases}\mathbf{R}_{ESS}\mathbf{y}_{P,ESS,\cdot|k} \leq \mathbf{1}V_{max} - \mathbf{V}^{n}_{\cdot|k}\\ \mathbf{1}V_{min} - \mathbf{V}^{n}_{\cdot|k} \leq \mathbf{R}_{ESS}\mathbf{y}_{P,ESS,\cdot|k}\end{cases} \tag{10}$$

— Box constraints:

$$b)\ -\mathbf{P}^{max}_{DG,k} - \mathbf{P}^{ref}_{DG,\cdot|k} \leq \mathbf{y}_{P,DG,\cdot|k} \leq 0 - \mathbf{P}^{ref}_{DG,\cdot|k},$$
$$c)\ \mathbf{Q}^{min}_{DG,k} - \mathbf{Q}^{ref}_{DG,\cdot|k} \leq \mathbf{y}_{Q,DG,\cdot|k} \leq \mathbf{Q}^{max}_{DG,k} - \mathbf{Q}^{ref}_{DG,\cdot|k},$$
$$d)\ \mathbf{P}^{min}_{ESS,k} - \mathbf{P}^{ref}_{ESS,k} \leq \mathbf{y}_{P,ESS,\cdot|k} \leq \mathbf{P}^{max}_{ESS,k} - \mathbf{P}^{ref}_{ESS,\cdot|k},$$
$$e)\begin{cases}\mathbf{SoC}^{min} - \mathbf{SoC}_{k-1} \leq H\mathbf{y}_{P,ESS,\cdot|k}\\ H\mathbf{y}_{P,ESS,\cdot|k} \leq \mathbf{SoC}^{max} - \mathbf{SoC}_{k-1}\end{cases} \tag{11}$$

B. SEPARATION OF THE PROBLEM

In this subsection, the separability of (9), (10) and (11) is analyzed, since the implementation of the MPC problem with the RSDD algorithm requires the objective function to be separable and the constraints to be formulated as function of a single node.

1) SEPARATION OF THE OBJECTIVE FUNCTION

Considering that the matrixes $\mathbf{W}_P$, $\mathbf{W}_Q$ and $\mathbf{W}_{SoC}$ are diagonals, the objective function can be written in a separable formulation for a single node $i \in N$ as follows:

$$\mathbf{Y}^{T}_{\cdot|k}[i] \cdot \mathbf{W}_{tot}[i,i] \cdot \mathbf{Y}_{\cdot|k}[i] + \mathbf{q}_{tot}[i] \cdot \mathbf{Y}_{\cdot|k}[i] \tag{12}$$

where $\mathbf{Y}_{\cdot|k}$ and $\mathbf{W}_{tot}[i,i]$ are the vector and diagonal matrix defined as:

$$\mathbf{Y}_{\cdot|k}[i] = \begin{bmatrix}\mathbf{y}_{P,DG,\cdot|k}[i] & \mathbf{y}_{Q,DG,\cdot|k}[i] & \mathbf{y}_{P,ESS,\cdot|k}[i]\end{bmatrix}^{T}$$
$$\mathbf{W}_{tot}[i] = \begin{bmatrix}\mathbf{W}_P[i,i] & 0 & 0\\ 0 & \mathbf{W}_Q[i,i],0 & \\ 0 & 0 & H^2\mathbf{W}_{SoC}[i,i]\end{bmatrix} \tag{13}$$

where:

- $[i]$ and $[i,i]$ describe the single element of the vector and of the diagonal respectively.

The vector $\mathbf{q}_{tot}[i]$ is defined as:

$$\mathbf{q}_{tot}[i] = 2\begin{bmatrix}0\\ 0\\ \mathbf{e}^{T}_{SoC,k-1}\mathbf{W}_{SoC}[i]\end{bmatrix}^{T} \tag{14}$$

2) SEPARATION OF THE COUPLING CONSTRAINTS

The coupling constraints defined in (10) are not directly separable, given that $\mathbf{R}_{DG}$, $\mathbf{X}_{DG}$ and $\mathbf{R}_{ESS}$ are full matrixes. However they can be separated considering each i-th column of the matrixes, as described in Appendix B-A. The resulting separated constraints for node $i \in N$ results in:

$$-\mathbf{g}_j(\mathbf{x}_j)_{|\forall j\neq i} \leq \mathbf{A}_C[i] \cdot \mathbf{Y}_{\cdot|k}[i] - \mathbf{b}^{-}_{C,k}[i]$$
$$\mathbf{A}_C[i] \cdot \mathbf{Y}_{\cdot|k}[i] - \mathbf{b}^{+}_{C,k}[i] \leq -\mathbf{g}_j(\mathbf{x}_j)_{|\forall j\neq i} \tag{15}$$

where the resulting matrixes $\mathbf{A}_C[i]$ and $\mathbf{b}^{+}_{C,k}[i]$, $\mathbf{b}^{-}_{C,k}[i]$ are defined in Appendix B-B, whereas the vector $\mathbf{g}_j(\mathbf{x}_j)$ describes the remaining part of the coupling constraints linked to the elements $j \neq i$ as described in Appendix B-A.

The box constraints in (11) are already separable, therefore they can be simply written in a compact form as follows:

$$\mathbf{b}^{-}_{B,k}[i] \leq \mathbf{A}_B[i] \cdot \mathbf{Y}_{\cdot|k}[i] \leq \mathbf{b}^{+}_{B,k}[i] \tag{16}$$

where the resulting matrixes $\mathbf{A}_B[i]$ and $\mathbf{b}^{+}_{B,k}[i]$, $\mathbf{b}^{-}_{B,k}[i]$ are defined in Appendix B-C. With this formulation, the right side and left side constraints are marked with the signs $+$ and $-$ respectively.

C. APPLICATION OF THE RSDD–MPC

The new formulation of the MPC composed of (12), (15) and (16) represents a constraint-coupled setup with convex optimization cost and convex constraints functions, given that the objective function and the constraints can expressed as a function of a single node $i \in N$. In fact, as demonstrated in [22], in the RSDD algorithm each agent i substitutes the term $\mathbf{g}_j(\mathbf{x}_j)$ of the coupling constraints with $\sum_{j\in P_i}(\boldsymbol{\lambda}^{ij} - \boldsymbol{\lambda}^{ji})$ and by means of relaxation the algorithm converges to a limit point feasible for the (not relaxed) coupling constraints (10) of the original problem. Therefore each node reconstructs the coupling constraints of the original optimization problem only based on the local measurements and predictions and on the exchange of the auxiliary variables $\left\{\boldsymbol{\lambda}^{ij}, \boldsymbol{\lambda}^{ji}\right\}_{j\in P_i}$.

The resulting application of the RSDD algorithm to the MPC problem, named RSDD–MPC, can be described for a node $i \in N$ with a set of neighbors $j \in P_i$ as follows:

1) OBJECTIVE FUNCTION

$$\sum_{s=1}^{\mathbf{N}_p}\mathbf{Y}^{T}_{\cdot|k}[i] \cdot \mathbf{W}_{tot}[i,i] \cdot \mathbf{Y}_{\cdot|k}[i]$$
$$+\mathbf{q}_{tot}[i] \cdot \mathbf{Y}_{\cdot|k}[i] + M\boldsymbol{\rho}_{tot,\cdot|k}[i] \tag{17}$$

where: $\boldsymbol{\rho}_{tot,k}[i] = [\boldsymbol{\rho}_{P,DG,k}[i], \boldsymbol{\rho}_{Q,DG,k}[i], \boldsymbol{\rho}_{P,ESS,k}[i]]$

2) COUPLING CONSTRAINTS

$$(+)\ \mathbf{A}_C[i] \cdot \mathbf{Y}_{\cdot|k}[i] - \boldsymbol{\rho}_{tot,\cdot|k}[i] \leq -\sum_{j\in P_i}(\boldsymbol{\lambda}^{ij,+}_{\cdot|k}(t+1)$$
$$-\boldsymbol{\lambda}^{ji,+}_{\cdot|k}(t+1)) + \mathbf{b}^{+}_{B,k}[i]$$
$$(-)\ -\sum_{j\in P_i}(\boldsymbol{\lambda}^{ij,-}_{\cdot|k}(t+1) - \boldsymbol{\lambda}^{ji,-}_{\cdot|k}(t+1)) + \mathbf{b}^{-}_{B,k}[i]$$
$$\leq \mathbf{A}_C[i] \cdot \mathbf{Y}_{\cdot|k}[i] - \boldsymbol{\rho}_{tot,\cdot|k}[i] \tag{18}$$

where:

- t is the iteration time of the algorithm
- The superscripts $+$ or $-$ specifies if the constraints functions are linked to the right or left side coupling constraints defined in (15).
- $\boldsymbol{\lambda}_{\cdot|k}^{ij,+/-} = [\boldsymbol{\lambda}_{P,DG,\cdot|k}^{ij,+/-}, \boldsymbol{\lambda}_{Q,DG,\cdot|k}^{ij,+/-}, \boldsymbol{\lambda}_{P,ESS,\cdot|k}^{ij,+/-}]$ are the neighboring variables linked to $+/-$ coupling constraints.
- $\boldsymbol{\lambda}_{\cdot|k}^{ij,+/-}(t+1) = \boldsymbol{\lambda}_{\cdot|k}^{ij,+/-}(t) + \gamma(\boldsymbol{\mu}_{\cdot|k}^{i,+/-}(t+1) - \boldsymbol{\mu}_{\cdot|k}^{j,+/-}(t+1))$
- $\boldsymbol{\mu}_{\cdot|k}^{i,+/-}$ and $\boldsymbol{\mu}_{\cdot|k}^{j,+/-}$ are the lagrangian multipliers linked to $+/-$ coupling constraints and related to node $i \in N$ and $j \in P_i$ respectively

3) BOX CONSTRAINTS

Since the box constraints defined in (16) are independent from the other neighbors, their formulation are identical to the one previously defined. Based on (7), an additional constraint for the variable $\boldsymbol{\rho}_{tot,k}[i]$ has to be defined as follows:

$$\boldsymbol{\rho}_{tot,\cdot|k}[i] \geq 0 \tag{19}$$

The variable $t \in 1, \ldots, t_{FIN}$, which appears also in Section III, represents the internal iteration of the algorithm, and differs from the time scale of the MPC problem s since it iterates during a single step of the MPC.

V. CALCULATION OF γ

This section presents a method to calculate the limits for the value of the parameter γ that guarantees the convergence of the RSDD algorithm. The calculation of the convergence condition is based on the Preposition 1.2.3 of [30] which states that given a function $f(x)$ and given a positive constant L that fulfils the *Lipschitz continuity* condition for $\nabla f(x)$:

$$\|\nabla f(x) - \nabla f(x')\| \leq L\|x - x'\| \tag{20}$$

the convergence of the gradient method is satisfied under the condition:

$$0 \leq \gamma \leq \frac{2}{L} \tag{21}$$

Following the demonstration of Preposition 6 of [5], the value of the constant L can be calculated based on the mean-value theorem, meaning that:

$$\|\nabla f(x) - \nabla f(x')\| \leq \|\nabla^2 f(x)\|\|x - x'\| \tag{22}$$

Given a generic separable problem defined as in Section III in (6), the RSDD algorithm is obtained by applying two successive duality steps from $f_i(x_i)$ to its dual $q_i(\boldsymbol{\mu}^i)$ and then from $q_i(\boldsymbol{\mu}^i)$ to $\eta_i(\{\lambda^{ij}, \lambda^{ji}\}_{j\in P_i})$ [22]. Based on the duality theory, the partial Lagrangian for the second dual problem is defined as:

$$\mathcal{L}(\boldsymbol{\mu}^1, \ldots, \boldsymbol{\mu}^N, \boldsymbol{\Lambda}) = \sum_{i=1}^{N}(q_i(\boldsymbol{\mu}^i) + \sum_{j\in P_i}\lambda^{ij}(\boldsymbol{\mu}^i - \boldsymbol{\mu}^j)) \tag{23}$$

Given that the calculation of λ^{ij} follows a gradient method (equation (14) in [22]), the convergence condition can be defined based on (21) and the value of the constant L can be calculated based on the mean-value theorem.

As described in [5], the *Lipschitz continuity* condition can be applied to the dual function (23), resulting in:

$$\|\nabla\mathcal{L}(\mathcal{M}^*, \boldsymbol{\Lambda}) - \nabla\mathcal{L}(\mathcal{M}^*, \boldsymbol{\Lambda}')\| \leq L\|\boldsymbol{\Lambda} - \boldsymbol{\Lambda}'\| \tag{24}$$

with $\mathcal{M}^* = (\boldsymbol{\mu}^{*,1}, \ldots, \boldsymbol{\mu}^{*,N})$ an optimal solution of the first dual step. Applying the mean-value theorem (22) results in:

$$\|\nabla\mathcal{L}(\mathcal{M}^*, \boldsymbol{\Lambda}) - \nabla\mathcal{L}(\mathcal{M}^*, \boldsymbol{\Lambda}')\| \leq \|\nabla^2\mathcal{L}(\boldsymbol{\mu}, \boldsymbol{\Lambda})\|\|\boldsymbol{\Lambda} - \boldsymbol{\Lambda}'\| \tag{25}$$

Given that the laplacian is a separable function [22], the calculation of the hessian can be performed using the formula presented in the Example 6.1.1 in [30]:

$$\begin{aligned}\nabla^2\mathcal{L}(\boldsymbol{\mu}^1, \ldots, \boldsymbol{\mu}^N, \boldsymbol{\Lambda}) &= \nabla^2\sum_i(q_i(\boldsymbol{\mu}^i) + \sum_j \lambda^{ij}n_i(\boldsymbol{\mu}^i, \boldsymbol{\mu}^j)) \\ &= -\sum_{i=1}^{N}\frac{N_i^T N_i}{\nabla^2 q_i(\boldsymbol{\mu}^i) + \sum_j \lambda^{ij}\nabla^2 n_{ij}(\boldsymbol{\mu}^i, \boldsymbol{\mu}^j)}\end{aligned} \tag{26}$$

where the vector $N_i = [\frac{\partial n_{i1}}{\boldsymbol{\mu}^i}, \ldots, \frac{\partial n_{ir}}{\boldsymbol{\mu}^i}]^T = \nabla_{\boldsymbol{\mu}^i}[(\boldsymbol{\mu}^i - \boldsymbol{\mu}^1), \ldots, (\boldsymbol{\mu}^i - \boldsymbol{\mu}^r)]^T$ with $1, \ldots, r \in P_i$. Therefore $N_i = \mathbf{1}^T$ with size $1, \ldots, r \in P_i$ and the product $N_i^T N_i = D[i, i]$, which is the diagonal element of the degree matrix D of the graph $\mathcal{G}$.

The denominator of (26) can be divided into the calculation of the two elements $\nabla^2 q_i(\boldsymbol{\mu}^i)$ and $\nabla^2 n_{ij}(\boldsymbol{\mu}^i, \boldsymbol{\mu}^j)$. From the calculation of N_i it is clear that the term $\nabla^2 n_{ij}(\boldsymbol{\mu}^i, \boldsymbol{\mu}^j)$ is null, whereas for the first element same approach used in (26) is applied.

Based on [22] the dual function $q_i(\boldsymbol{\mu}^i)$ is defined as $f_i(x_i) + \sum_s \boldsymbol{\mu}^s g_{is}(x_i)$, meaning that the calculation of the hessian results in:

$$\nabla^2 q(\mathbf{x}, \boldsymbol{\mu})[i] = -\frac{G_i^T G_i}{\nabla^2 f_i(x_i) + \sum_s \boldsymbol{\mu}^s \nabla^2 g_{is}(x_i)} \tag{27}$$

where $G_i = [\frac{\partial g_{1i}}{x_i}, \ldots, \frac{\partial g_{mi}}{x_i}]$.

In case the constraints are expressed as:

$$\mathbf{A}\cdot\mathbf{x} \leq \mathbf{b}; \begin{bmatrix} a_{11}, & \ldots & a_{1n} \\ \vdots & \vdots & \vdots \\ a_{m1}, & \ldots & a_{mn} \end{bmatrix} \cdot \begin{bmatrix} x_1 \\ \vdots \\ x_n \end{bmatrix} - \begin{bmatrix} b_1 \\ \vdots \\ b_n \end{bmatrix} \leq [0]_{n\times 1} \tag{28}$$

each term $G_i = [a_{1i}, \ldots, a_{mi}]^T$ and the product $G_i^T G_i = A^T A[i, i]$, that is the element i of the diagonal of $A^T A$. As for (26), the calculation of the denominator of (27) can be divided into te calculation of $\nabla^2 f_i(x_i)$ and $\nabla^2 g_{is}(x_i)$, where in case the constraints are formulated as in (28), the term $\nabla^2 g_{is}(x_i)$ is null. If the function f_i is a quadratic separable function described as $\frac{1}{2}\mathbf{x}^T\mathbf{W}\mathbf{x}$ where $\mathbf{W}$ is a diagonal matrix of elements $[w_1, \ldots, w_n]$, then the term $\nabla^2 f_i(x_i) = w_i$.

Based on [30], the hessian of the lagrangian of a separable problem is a diagonal matrix, therefore the resulting hessian

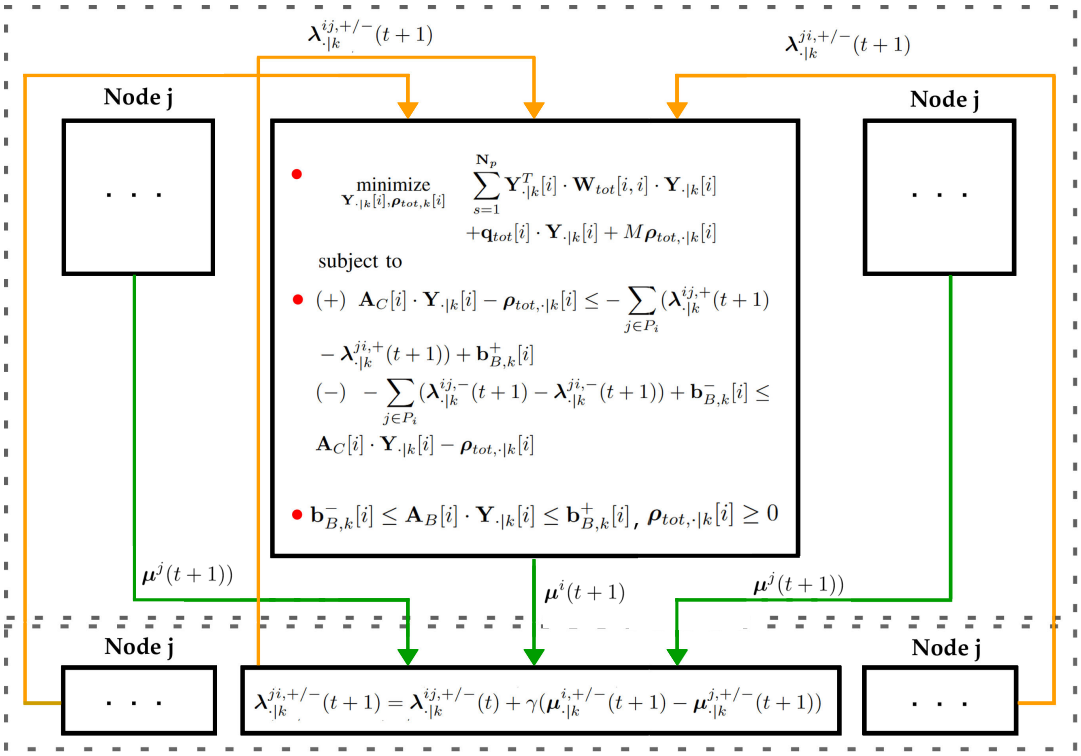

FIGURE 1. Scheme of the RSDD–MPC.

of the lagrangian $\mathcal{L}(\boldsymbol{\mu}^1, \ldots, \boldsymbol{\mu}^N, \boldsymbol{\Lambda})$ is a diagonal matrix $\boldsymbol{H}$ whose elements $[i, i]$ on the diagonal are defined as:

$$\boldsymbol{H}[i,i] = \frac{D[i,i]}{\nabla^2 q(\mathbf{x}, \boldsymbol{\mu}^1, \ldots, \boldsymbol{\mu}^N)[i]} = \frac{D[i,i] \cdot w_i}{A^T A[i,i]} \quad (29)$$

Given that norm-2 of a symmetric matrix is equal to its spectral radius, the mean-value theorem can be reformulated as follows:

$$\|\nabla\mathcal{L}(\mathcal{M}^*, \boldsymbol{\Lambda}) - \nabla\mathcal{L}(\mathcal{M}^*, \boldsymbol{\Lambda}')\| \leq \rho(\boldsymbol{H})\|\boldsymbol{\Lambda} - \boldsymbol{\Lambda}'\| \quad (30)$$

meaning that for (21), the convergence condition for γ can be defined as:

$$0 \leq \gamma \leq \frac{2}{\rho(\boldsymbol{H})} \quad (31)$$

Equation (31) shows that the upper limits of the control parameter γ depends on matrix A, which, in the proposed control application, represents the resistance and reactance matrix of the grid, described in Section II-B. Therefore, using the grid information, equation (31) guarantees the convergence of the RSDD algorithm.

VI. SIMULATION AND RESULTS

A. SIMULATION SCENARIO

The grid model used for the simulation is composed of $N_{tot} = 26$ nodes, described in Figure 2. Table 1 shows the data used for the lines, in terms of per unit (p.u.) values of resistance and reactance, where the nominal voltage is set as $\mathbf{V}_{nom} = 380\ V$ and nominal power as $\mathbf{P}_{nom} = 4\,\text{kW}$.

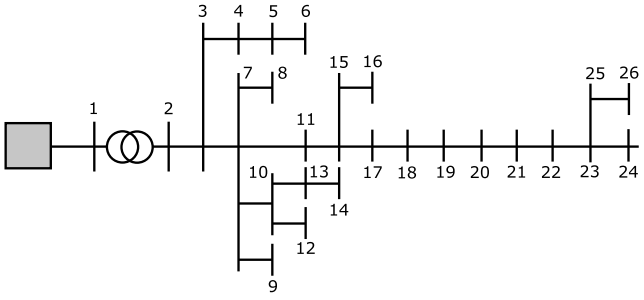

FIGURE 2. 26-nodes distribution grid used for the simulation.

The tests performed in this section can be divided in three groups as follows:

- *Test of the convergence condition* : The first set of tests have been implemented to validate the calculation of $\gamma_{limit} = \frac{2}{\rho(\boldsymbol{H})}$ defined in (31). In the tests, load and generation profiles are considered fixed while both PVs (which substitute the generic DGs) and ESSs are assigned to a set of nodes. To validate γ_{limit}, first a series of simulations is run with different values of γ to show that the algorithm does not converge when the limit value is exceeded, then a set of simulations is run with a fixed value of γ but with different number of PVs and ESSs installed to show that the (31) is valid for different problem size.
- *Test of the RSDD–MPC*: The third set of tests have been performed to test the ability of the RSDD–MPC,

TABLE 1. Distribution grid data.

Start	End	Per unit resistance	Per unit reactance	Start	End	Per unit resistance	Per unit reactance
1	2	0.001	0.003172	11	15	0.000905625	0.00034125
2	3	0.00108675	0.0004095	15	16	0.000802125	0.00030225
3	4	0.0004269375	0.000160875	15	17	0.000336375	0.00012675
4	5	0.00087975	0.0003315	17	18	0.0006598125	0.000248625
5	6	0.0009315	0.000351	18	19	0.0005304375	0.000199875
3	7	0.00013584375	0.000511875	19	20	0.0008150625	0.000307125
7	8	0.0000388125	0.000014625	20	21	0.000336375	0.00012675
7	9	0.0006856875	0.000258375	21	22	0.00025875	0.0000975
7	10	0.00098325	0.0003705	22	23	0.0004528125	0.000170625
7	11	0.0007115625	0.000268125	23	24	0.000336375	0.00012675
10	12	0.00098325	0.0003705	23	25	0.00025875	0.0000975
10	13	0.0007245	0.000273	25	26	0.0004528125	0.000170625
13	14	0.000414	0.000156				

configured with a fixed number of iterations, to control the voltage and to track the power and SoC references in terms of the percentage of error with the centralized solution. In all the tests, load and generation profiles are considered fixed while both PVs and ESSs are assigned to a set of nodes. First a set of simulations have been run in an overvoltage scenario with eventually active or reactive power references to track, then, in a normal voltage condition, a reference for the SoC has been provided to the RSDD–MPC.

- *Test with realistic load and generation profiles*: The final set of tests have been performed considering realistic load and generation profiles during 24 hours with ESSs and PVs assigned to the same set of nodes as in *Test of the RSDD–MPC*.

Both in *Test of the convergence condition* and *Test of the RSDD–MPC* the nominal power of the PVs have been considered equal to 1 p.u. each whereas loads and ESSs have a nominal power of 0.875 p.u., which have been calculated based on $\mathbf{P}_{nom}$. In *Test with realistic load and generation profiles* the PV profiles have been calculated considering 1 p.u. as nominal power. As mentioned in Section IV, each customer $i \in N$ with N less or equal to the total number of nodes N_{tot} is equipped with both PV and ESS.

B. NUMERICAL RESULTS

In this section, simulation results are used to demonstrate the condition for γ_{limit} described in Section V and the convergence of the RSDD–MPC described in Section IV. In both cases, the results obtained with the RSDD are compared with the simulations obtained with the OSQP solver ([31]) applied in a centralized manner that performs the MPC problem described in Section II-B. The power flow simulation of the electrical grid has been conducted by means of PYPOWER [32]. In all the tests and for both the centralized and the RSDD–MPC formulations, the values used for the weighting matrixes are the following:

$$\mathbf{W}_P = \mathbf{W}_Q = \mathbf{W}_{SoC} = \mathbb{I} \tag{32}$$

For each simulation, the graph $\mathcal{G}$ is determined based on the nodes where PVs and ESSs have been assigned, considering that each node is linked only to its two nearest neighbors.

1) TEST OF THE CONVERGENCE CONDITION

The first numerical simulation is performed to demonstrate the calculation of the limit for the value of γ in (31). The test considers the grid model defined in Section VI-A where both PVs and ESSs have been assigned to nodes [3, 5, 8, 9, 12, 15, 16, 18, 19, 20, 21, 24, 26]. For the sake of simplicity, in this first test only the reactive power control is considered, given that the focus of the test is to prove the convergence condition for γ.

The generation of all the PVs have been set to $\mathbf{P}^{max}_{DG,k} = 1$ p.u, whereas the load value of each node is equal to 0.33 p.u. so as to produce a voltage rise in some of the nodes of the grid. Based on the aforementioned configuration, the gamma limit for the voltage control is calculated based on (31) resulting in:

$$\gamma_{lim} = 4.9815 \times 10^{-6} \tag{33}$$

The value of M has been selected $M = 100$, high enough to satisfy condition on Theorem II.6 defined in [22].

Based on the calculated value of γ_{limit} the first test has been accomplished by performing the RSDD algorithm with values of $\gamma = k \cdot \gamma_{lim}$ where $k = [0.0125, 0.025, 0.05, 0.125, 0.25, 0.375, 0.5, 0.625, 0.75, 1.0, 1.5, 2.5]$. For each value of γ, $t_{FIN} = 300$ RSDD iterations are performed and at the end of the simulation the error with the previous calculated centralized version is evaluated by dividing the average value of the difference between the distributed and the centralized solution and the average value of the centralized solution as follows:

$$RSDD_{error} = \frac{\overline{\mathbf{Y}_{k,RSDD}(t_{FIN}) - \mathbf{Y}_{k,Cent}}}{\overline{\mathbf{Y}_{k,Cent}}} \cdot 100 \tag{34}$$

The structure of the test is described in Figure 3, which shows that the result of a single iteration of the power flow is used to calculate both the centralized and the RSDD solution.

The result of the test is described in Figure 4, where the RSDD error is compared for each value of γ.

From the figure it appears clear that for values higher than γ_{lim} (blue dashed line in the figure), the RSDD error tends to rapidly increase, eventually reaching the point where the algorithm is not able to converge. The figure also shows that for very small values of γ the error is relatively large,

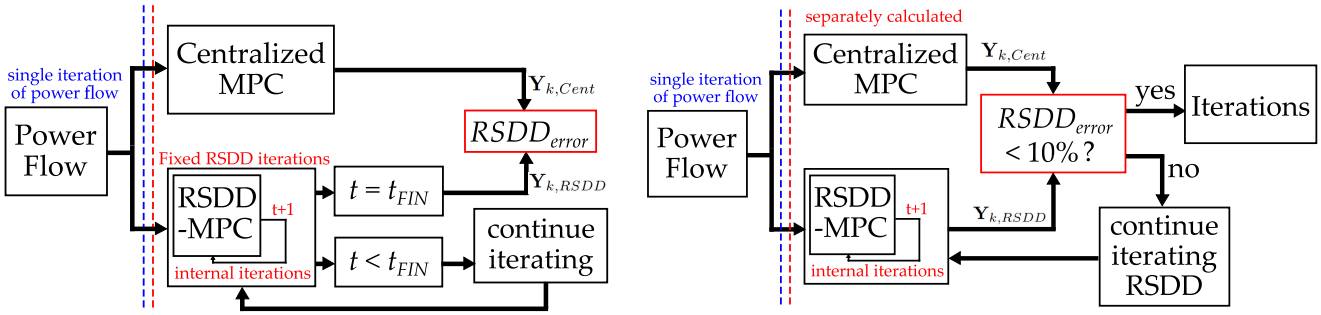

(a) Simulation setup for the first test of the convergence condition

(b) Simulation setup for the second test for the convergence condition

FIGURE 3. Test of the convergence condition.

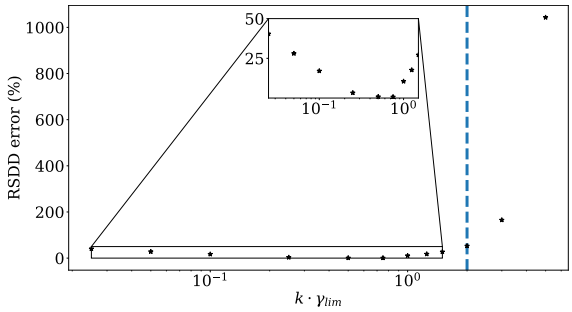

FIGURE 4. Result of the first test for the convergence condition.

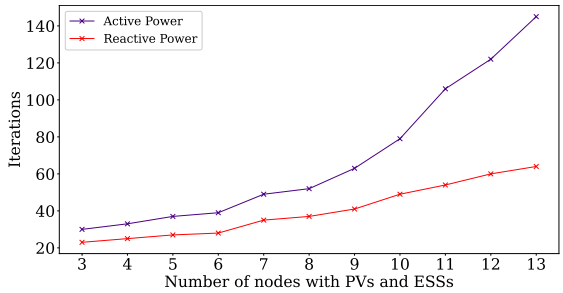

FIGURE 5. Result of the second test for the convergence condition.

which demonstrates that with small values of the step-size the convergence speed is so slow that 300 iterations are not sufficient to reach an acceptable result.

The second test for the convergence condition is performed using a fixed value of $\gamma = 0.5 \cdot \gamma_{lim}$, given that, based on Figure 4, the minimum values of the error are obtained with $0.5 \leq \gamma_{lim} < 1$. In the test, both active and reactive power control set-points are considered and the number of nodes in the grid with installed PVs and ESSs are increased from the list of nodes defined previously, starting with only 4 nodes and reaching at the end the full list. Therefore, in this case γ_{lim} is a vector calculated using matrix $\mathbf{R}_{DG}$ and $\mathbf{X}_{DG}$ for active and reactive power respectively. In the structure of the test described in Figure 3b the RSDD continues internally iterating until the RSDD error is less than 10%.

The result of this test is described in Figure 5, which shows that the number of iterations increases almost linearly with the number of nodes. In particular, the figure shows that the control of the active power, given the same number of nodes, requires more time to converge to an error less than 10% in comparison with the reactive power control.

Both tests have demonstrated that the choice of the value for γ has a considerable impact on the convergence of the algorithm, which also is confirmed by (8), given that γ defines the step-size for the update of the neighboring variables. Besides, the number of controllable nodes influences the number of iterations required to reach an acceptable error with the centralized formulation. Although the size of the problem is taken into account in the calculation of γ (matrix $\mathbf{A}$), once the value of k is fixed, the speed of convergence of the algorithm is only affected by the number of nodes.

Figure 5 highlights a limitation of the proposed RSDD–MPC approach, since the linear increase of the number of iterations represents a potential challenge in terms of scalability. Some distributed algorithms have tried to overcome this problem, e.g., in [5], where values of lagrangian multipliers related to power limits are used to reduce the number of nodes actively involved in solving the overvoltage. The solution presented in [5] might be tested with the proposed RSDD–MPC to reduce the number of iterations, since both controllers are based on dual theory and exchange auxiliary variables among the control nodes.

2) TEST OF THE RSDD–MPC

The results of the simulations performed in this subsection are used to compare the control output of the RSDD–MPC with the solution obtained with the centralized formulation in terms of the ability to generate a control output closer to the centralized solution and to track a reference with the MPC predictions. For the simulations, the values $t_{FIN} = 200$ and $\gamma = 0.5 \cdot \gamma_{lim}$ have been selected based on the outcome of the tests in Section VI-B1. The value $M = 100$ has been selected to satisfy Theorem II.6 defined in [22]. The structure of the first test is described in Figure 6a where, similarly to Figure 3b, one iteration of the power flow is used to calculate both the centralized and the RSDD solutions, therefore only

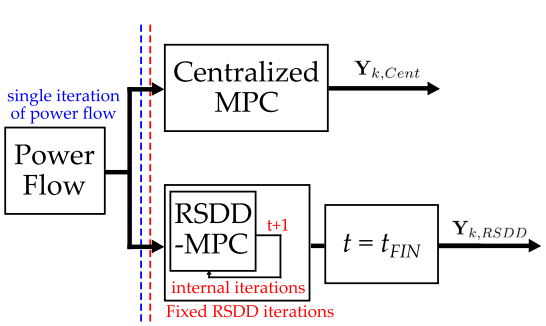

(a) Simulation setup for the RSDD–MPC

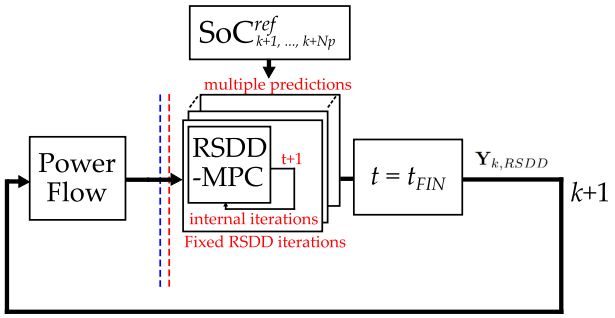

(b) Simulation setup for the RSDD–MPC with multiple power flow iterations

FIGURE 6. **Test of the RSDD–MPC.**

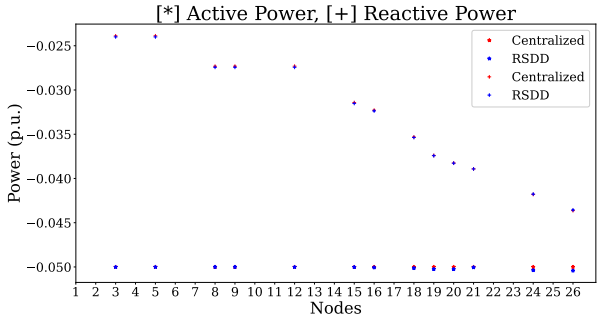

(a) Active power tracking and Reactive power control

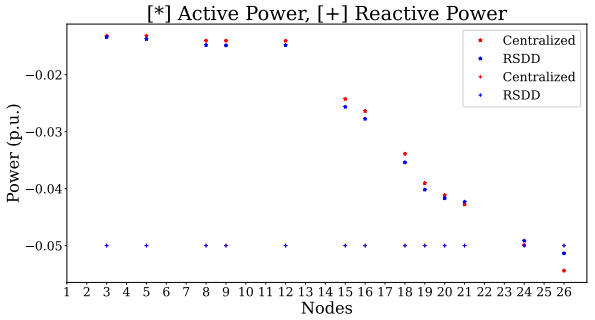

(b) Active power curtailment and Reactive power tracking

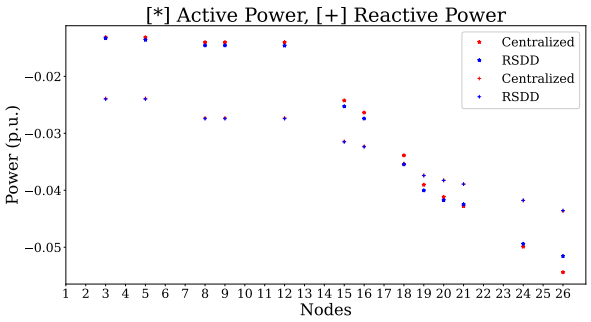

(c) Active power and Reactive power control

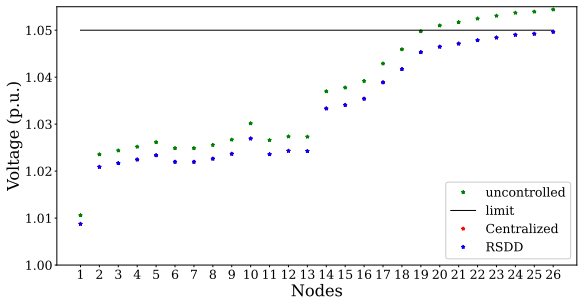

(d) Voltage of the nodes

FIGURE 7. **Simulation results for the test with only voltage reference.**

the first prediction of the MPC is taken into account. The test has been performed with the same group of selected nodes and the generation and load conditions of Subsection VI-B1. The load value has been set equal to $\mathbf{P}^{load}_{k} = 0.33$ (p.u.) and the generation equal to $\mathbf{P}^{max}_{DG,k} = 1.0$. This load and generation conditions produce an overvoltage in the simulated grid, exceeding therefore the coupling constraints for the voltage. The RSDD–MPC has been applied to the simulated grid with three different configurations:

- a) With a active power reference $\mathbf{P}^{ref}_{DG,k} = -0.05$ (p.u.)
- b) With a reactive power reference $\mathbf{Q}^{ref}_{DG,k} = -0.05$ (p.u.)
- c) Without active or reactive power references

In all the three cases, the control of the active power of the ESSs has been disabled given that the focus will be given on second test of this subsection.

The results of the first prediction of the MPC, meaning for $s = 1$, are depicted in Figure 7a, 7b, 7c where the active and reactive power outputs of the PVs obtained by the Centralized and RSDD formulations are compared for the case a), b) and c) respectively. To differentiate the results for the reactive power and the active power injections, the symbol $+$ and $*$ are used accordingly. The resulting voltage profile, identical for the three cases, is described in Figure 7d, which shows that the calculated control outputs shift the voltage of the nodes below the upper limit value. Figures 7a, 7b, 7c highlights how the results of the RSDD–MPC using a limited number of iteration t_{FIN} achieve a solution that is close to the centralized one. The error among the centralized and the distributed solutions can be reduced by increasing of the number of iterations. Moreover, the test also shows in Figure 7a and 7b that the RSDD–MPC is able to track the references

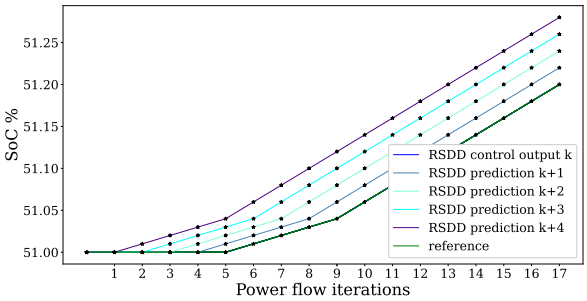

(a) Tracking of the reference for the SoC

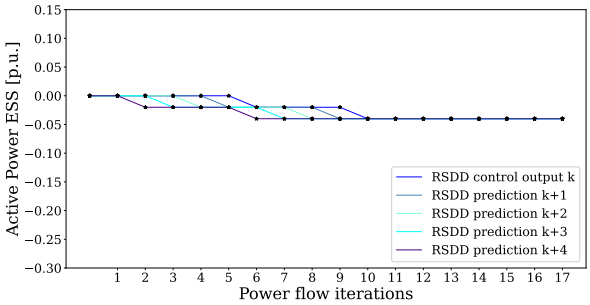

(b) Result of the Active Power ESSs for the tracking of the SoC

FIGURE 8. Simulation results for the test with SoC reference.

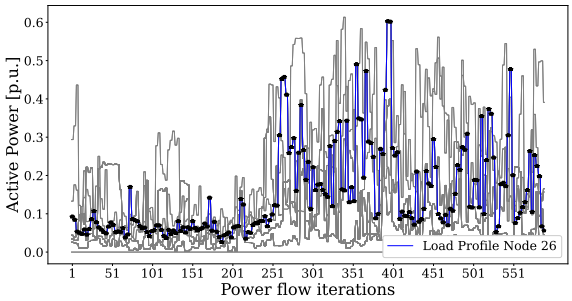

(a) Load profiles

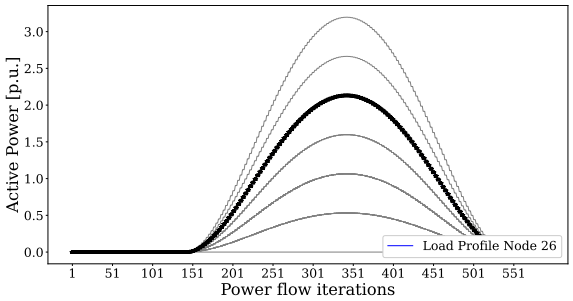

(b) Generation profiles with clean sky conditions

FIGURE 9. 24 hours load and generation profiles.

and to use the remaining available resources to satisfy the constraints.

The second test has been performed to prove the ability of the RSDD–MPC to track the SoC reference value, which in the RSDD formulation is part of $\mathbf{q}_{tot}$ and it is described in $\mathbf{e}_{SoC,k-1}$ of Appendix A, whereas for the centralized formulation the SoC reference is part of (3). In the test the other reference values $\mathbf{P}^{ref}_{DG,k}, \mathbf{Q}^{ref}_{DG,k}, \mathbf{P}^{ref}_{ESS,k}$ are null and the load value has been set to $\mathbf{P}^{load}_{k} = 0.4$ (p.u.), so that the voltage does not exceed the limit. By doing so, the results only prove the tracking capability of the SoC, excluding the activation of the control of the voltage or the tracking of the other variables. The simulation setup is described in Figure 6b, which shows that the result of the RSDD–MPC is used as input for a new iteration $k+1$ of the power flow. To calculate the predicted values, the reference values $\mathbf{SoC}^{ref}_{\cdot|k}$ are provided to the MPC with $N_p = 4$ the number of predictions. The result of the numerical simulation described in Figure 8a highlights the ability the RSDD–MPC to track the SoC reference, which from the value of 51% at iteration 5 goes to value of 51.05% at iteration 9 and then to value of 51.20% at iteration 17 with a difference charging rate. The Figure also shows that the resulting predictions calculated by the algorithm are able to predict the output of the successive iterations. The resulting active power control outputs for the ESSs required to track the SoC are described in Figure 8b. The figure shows that the control output for the ESSs until iteration 5 is zero because there is no change in the SoC reference. Starting from iteration 5 the ESSs starts absorbing active power in order to increase their SoC and thus being able to track the reference. After iteration 10, the active power changes value required to maintain a different charging slope. The Figure also shows that the RSDD–MPC is able to predict the resulting active power output.

3) TEST WITH REALISTIC LOAD AND GENERATION PROFILES

An additional series of tests have been performed considering 24 hours load and generation profiles, to show the performance of the proposed control strategy with realistic scenarios. The profiles used for the simulation are described in Figure 9, where the ones assigned to Node 26 are highlighted in blue. The control parameters have been selected identical to the ones used in *Test of the RSDD–MPC*.

Figure 9a shows the load profiles obtained with the tool developed in the Flexmeter project [33] and used for the simulation test. The profiles exhibit high fluctuations, which are typical in realistic Low Voltage (LV) distribution grids [28]. The generation profiles in Figure 9b represent a typical clean sky condition, which in terms of overvoltage scenarios is the most critical. The profiles were calculated using the tool described in [34] considering a day in August and assuming the position of the distribution grid in the coordinates N50°77′ E6°9′ (corresponding to the city of Aachen, Germany). The profiles consider different level of power

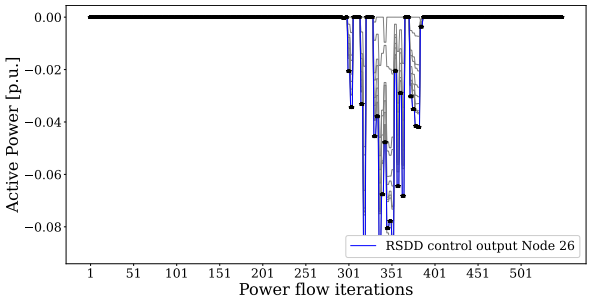

(a) Active power set-points with RSDD control

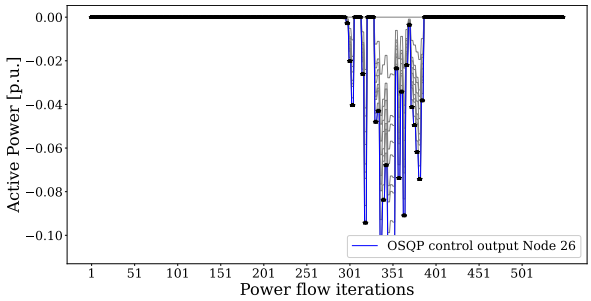

(b) Active power set-points with Centralized control

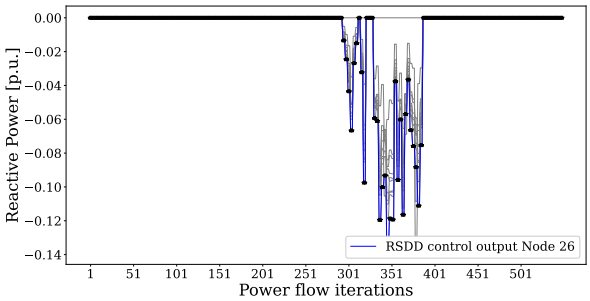

(c) Reactive power set-points with RSDD control

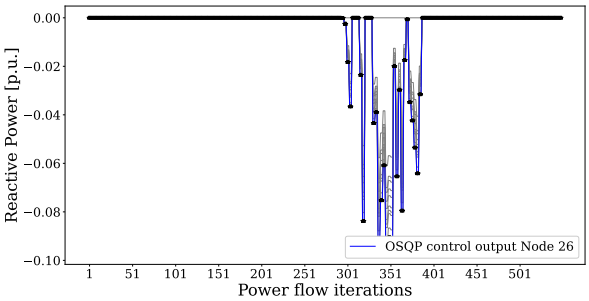

(d) Reactive power set-points with Centralized control

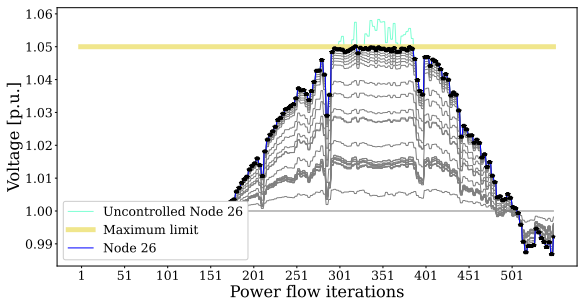

(e) Voltage profiles resulting from RSDD control

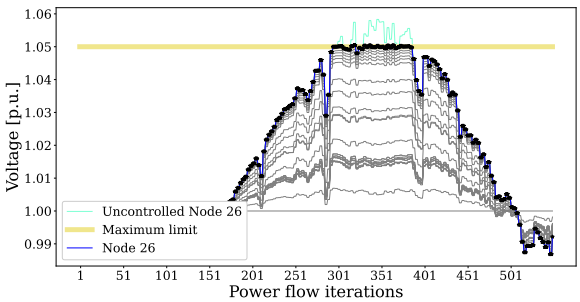

(f) Voltage profiles resulting from Centralized control

FIGURE 10. **Simulation results with 24 hours profiles.**

installation which could be lower or higher than the nominal power.

The results of the simulation tests are described in Figure 10, where the application of the RSDD–MPC, on the left side, is compared with the application of the centralized control on the right side. Both control strategies are able to solve the overvoltage problem (highlighted with light green curve) by calculating the active and reactive power set-points of the DGs for the 24 hours simulation. However, although the voltage profile obtained with the RSDD–MPC is equal to the voltage profile resulting from the centralized control, the active and reactive set-points profiles show different behaviors. This difference is nevertheless quite limited, given that the changes in the power absorption show the same dynamics. Therefore, even if RSDD–MPC, with the selected value of t_{FIN}, does not reach the same optimal solution as the centralized approach, the difference remains acceptable for the voltage control purpose.

VII. CONCLUSION

This paper presents the constraint-coupled MPC problem for voltage control applied to distribution grid solved with the RSDD algorithm. The MPC optimization problem has been first reformulated from its centralized expression in the constraint-coupled set-up and subsequently the RSDD–MPC algorithm has been derived. For the algorithm, the convergence condition for the limit value of the step-size is derived. Numerical simulations have validated the calculation of the limit value of step-size, which depends only on the size of the problem and on the grid data. However, the simulations have also demonstrated a limitation of the RSDD–MPC due to the linear increase in the number of iterations as the number of control nodes increases. The comparison with the results obtained from the solution of the centralized MPC shows that the RSDD–MPC solves the MPC problem in a distributed manner and with a fixed number of iterations, reaching a solution that is closer to the centralized one. Moreover, additional

simulations demonstrate that the RSDD–MPC tracks reference values for the SoC over a finite prediction horizon. The proposed application of the RSDD represents an interesting option for implementing a distributed voltage control over a prediction horizon using an algorithm with a simple structure and a demonstrated calculation of the limit value of the step-size. A further improvement to the RSDD–MPC could involve finding a method for solving the scalability problem.

APPENDIX A
NEW VARIABLE FORMULATION

- $\mathbf{y}_{P,DG,\cdot|k} = (\mathbf{P}^{curt}_{DG,\cdot|k} - \mathbf{P}^{ref}_{DG,\cdot|k})$
- $\mathbf{y}_{Q,DG,\cdot|k} = (\mathbf{Q}_{DG,\cdot|k} - \mathbf{Q}^{ref}_{DG,\cdot|k})$
- $\mathbf{y}_{P,ESS,\cdot|k} = (\mathbf{P}_{ESS,\cdot|k} - \mathbf{P}^{ref}_{ESS,\cdot|k})$
- $\mathbf{e}_{SoC,k-1} = (\mathbf{SoC}_{k-1} - \mathbf{SoC}^{ref}_{k-1})$
- $H = \frac{\eta}{\mathbf{C}_{ESS}}$

APPENDIX B
SEPARATION OF THE CONSTRAINTS

A. GENERAL SEPARATION THEORY

Given a set of constraints that can be expressed as follows:

$$\mathbf{A} \cdot \mathbf{x} \leq \mathbf{b} \tag{35}$$

where $\mathbf{A}$ is a full $n \times n$ matrix and $\mathbf{x}$, $\mathbf{b}$ two $1 \times n$ vectors, they can be reformulated as follows:

$$\begin{cases} a_{11}x_1 + \ldots + a_{1j}x_j + \ldots + a_{1n}x_n \leq \mathbf{1}^T \dfrac{b_1}{n} \\ \vdots \\ a_{i1}x_1 + \ldots + a_{ij}x_j + \ldots + a_{1n}x_n \leq \mathbf{1}^T \dfrac{b_1}{n} \\ \vdots \\ a_{n1}x_1 + \ldots + a_{nj}x_j + \ldots + a_{nn}x_n \leq \mathbf{1}^T \dfrac{b_n}{n} \end{cases} \tag{36}$$

Therefore the constraint linked to the r-th element of $\mathbf{x}$ can be defined as:

$$\begin{cases} a_{1r}x_r - \dfrac{b_1}{n} \leq \underbrace{-a_{11}x_1 + \dfrac{b_1}{n} - \ldots - a_{1n}x_n + \dfrac{b_1}{n}}_{-g_{1j}(\mathbf{x}_j)|\forall j \neq r} \\ \vdots \\ a_{ir}x_r - \dfrac{b_i}{n} \leq \underbrace{-a_{i1}x_1 + \dfrac{b_i}{n} - \ldots - a_{in}x_n + \dfrac{b_i}{n}}_{-g_{ij}(\mathbf{x}_j)|\forall j \neq r} \\ \vdots \\ a_{nr}x_r - \dfrac{b_n}{n} \leq \underbrace{-a_{n1}x_1 + \dfrac{b_n}{n} - \ldots - a_{nn}x_n + \dfrac{b_n}{n}}_{-g_{nj}(\mathbf{x}_j)|\forall j \neq r} \end{cases} \tag{37}$$

and in its compact form as:

$$\mathbf{g}_r(x_r) = \begin{bmatrix} a_{1r} \\ \vdots \\ a_{nr} \end{bmatrix} \cdot x_r - \begin{bmatrix} \frac{b_1}{n} \\ \vdots \\ \frac{b_n}{n} \end{bmatrix} \leq \begin{bmatrix} -g_{1j}(\mathbf{x}_j) \\ \vdots \\ -g_{nj}(\mathbf{x}_j) \end{bmatrix} = -\mathbf{g}_j(\mathbf{x}_j)|\forall j \neq r \tag{38}$$

B. RESULTING I-TH ELEMENT OF $\mathbf{A}_C$ AND $\mathbf{b}^+_{C,k}, \mathbf{b}^-_{C,k}$

The separated constraints for the element i-th $\in N$ are described as:

$$\mathbf{A}_C[i] = \begin{bmatrix} \mathbf{R}_{DG}[1,i] & 0 & 0 \\ \vdots & \vdots & \vdots \\ \mathbf{R}_{DG}[N,i] & 0 & 0 \\ 0 & \mathbf{X}_{DG}[1,i] & 0 \\ \vdots & \vdots & \vdots \\ 0 & \mathbf{X}_{DG}[N,i] & 0 \\ 0 & 0 & \mathbf{R}_{ESS}[1,i] \\ \vdots & \vdots & \vdots \\ 0 & 0 & \mathbf{R}_{ESS}[N,i] \end{bmatrix} \tag{39}$$

$$\mathbf{b}^+_{C,k}[i] = \begin{bmatrix} \left[\dfrac{\mathbf{1}V_{max} - \mathbf{V}^n_k[i]}{N}\right]_{1\times N} \\ \left[\dfrac{\mathbf{1}V_{max} - \mathbf{V}^n_k[i]}{N}\right]_{1\times N} \\ \left[\dfrac{\mathbf{1}V_{max} - \mathbf{V}^n_k[i]}{N}\right]_{1\times N} \end{bmatrix} \tag{40}$$

$$\mathbf{b}^-_{C,k}[i] = \begin{bmatrix} \left[\dfrac{\mathbf{1}V_{min} - \mathbf{V}^n_k[i]}{N}\right]_{1\times N} \\ \left[\dfrac{\mathbf{1}V_{min} - \mathbf{V}^n_k[i]}{N}\right]_{1\times N} \\ \left[\dfrac{\mathbf{1}V_{min} - \mathbf{V}^n_k[i]}{N}\right]_{1\times N} \end{bmatrix} \tag{41}$$

C. RESULTING I-TH ELEMENT OF $\mathbf{A}_B$ AND $\mathbf{b}^+_{B,k}, \mathbf{b}^-_{B,k}$

$$\mathbf{A}_B[i] = \begin{bmatrix} 1 & 0 & 0 \\ 0 & 1 & 0 \\ 0 & 0 & 1 \\ 0 & 0 & H \end{bmatrix} \tag{42}$$

$$\mathbf{b}^+_{B,k}[i] = \begin{bmatrix} 0 - \mathbf{P}^{ref}_{DG,k} \\ \mathbf{Q}^{max}_{DG,k} - \mathbf{Q}^{ref}_{DG,k} \\ \mathbf{P}^{max}_{ESS,k} - \mathbf{P}^{ref}_{ESS,k} \\ \mathbf{SoC}^{max} - \mathbf{SoC}_{k-1} \end{bmatrix} \tag{43}$$

$$\mathbf{b}^-_{B,k}[i] = \begin{bmatrix} -\mathbf{P}^{max}_{DG,k} - \mathbf{P}^{ref}_{DG,k} \\ \mathbf{Q}^{min}_{DG,k} - \mathbf{Q}^{ref}_{DG,k} \\ \mathbf{P}^{min}_{ESS,k} - \mathbf{P}^{ref}_{ESS,k} \\ \mathbf{SoC}^{min} - \mathbf{SoC}_{k-1} \end{bmatrix} \tag{44}$$

REFERENCES

[1] *Voltage Characteristics of Electricity Supplied by Public Electricity Networks*, Standard EN 50160, 2010.

[2] *IEEE Standard for Interconnection and Interoperability of Distributed Energy Resources With Associated Electric Power Systems Interfaces*, Standard 1547-2018 (Revision IEEE Std 1547-2003), IEEE, Apr. 2018, pp. 1–138.
[3] K. Turitsyn, P. Sulc, S. Backhaus, and M. Chertkov, "Options for control of reactive power by distributed photovoltaic generators," *Proc. IEEE*, vol. 99, no. 6, pp. 1063–1073, Jun. 2011.
[4] Y. W. Li and C.-N. Kao, "An accurate power control strategy for power-electronics-interfaced distributed generation units operating in a low-voltage multibus microgrid," *IEEE Trans. Power Electron.*, vol. 24, no. 12, pp. 2977–2988, Dec. 2009.
[5] S. Bolognani, R. Carli, G. Cavraro, and S. Zampieri, "On the need for communication for voltage regulation of power distribution grids," *IEEE Trans. Control Netw. Syst.*, vol. 6, no. 3, pp. 1111–1123, Sep. 2019.
[6] E. Commision. *Digitalisation of the Energy Sector*. Accessed: Sep. 22, 2021. [Online]. Available: http://ec.europa.eu/energy/topics/technology-and-innovation/digitalisation-of-the-energy-sector
[7] M. Pau, E. De Din, F. Ponci, P. A. Pegoraro, S. Sulis, and C. Muscas, "Impact of uncertainty sources on the voltage control of active distribution grids," in *Proc. Int. Conf. Smart Energy Syst. Technol. (SEST)*, Sep. 2021, pp. 1–6.
[8] F. Shariatzadeh, S. Chanda, A. K. Srivastava, and A. Bose, "Real-time benefit analysis and industrial implementation for distribution system automation and control," *IEEE Trans. Ind. Appl.*, vol. 52, no. 1, pp. 444–454, Jan. 2016.
[9] M. Vadari, R. Melton, and K. Schneider, "Distribution operations: The evolution of distributed energy resources [guest editorial]," *IEEE Power Energy Mag.*, vol. 18, no. 1, pp. 14–16, Jan. 2020.
[10] M. Farivar, R. Neal, C. Clarke, and S. Low, "Optimal inverter VAR control in distribution systems with high PV penetration," in *Proc. IEEE Power Energy Soc. Gen. Meeting*, Jul. 2012, pp. 1–7.
[11] T. Niknam, M. Zare, and J. Aghaei, "Scenario-based multiobjective Volt/VAR control in distribution networks including renewable energy sources," *IEEE Trans. Power Del.*, vol. 27, no. 4, pp. 2004–2019, Oct. 2012.
[12] E. Dall'Anese, S. S. Guggilam, A. Simonetto, Y. C. Chen, and S. V. Dhople, "Optimal regulation of virtual power plants," *IEEE Trans. Power Syst.*, vol. 33, no. 2, pp. 1868–1881, Mar. 2018.
[13] A. Nedic, A. Ozdaglar, and P. A. Parrilo, "Constrained consensus and optimization in multi-agent networks," *IEEE Trans. Autom. Control*, vol. 55, no. 4, pp. 922–938, Apr. 2010.
[14] M. Zhu and S. Martinez, "On distributed convex optimization under inequality and equality constraints," *IEEE Trans. Autom. Control*, vol. 57, no. 1, pp. 151–164, Jan. 2012.
[15] D. K. Molzahn, F. Dörfler, H. Sandberg, S. H. Low, S. Chakrabarti, R. Baldick, and J. Lavaei, "A survey of distributed optimization and control algorithms for electric power systems," *IEEE Trans. Smart Grid*, vol. 8, no. 6, pp. 2941–2962, Nov. 2017.
[16] P. Li, C. Zhang, Z. Wu, Y. Xu, M. Hu, and Z. Dong, "Distributed adaptive robust Voltage/VAR control with network partition in active distribution networks," *IEEE Trans. Smart Grid*, vol. 11, no. 3, pp. 2245–2256, May 2020.
[17] E. De Din, F. Bigalke, M. Pau, F. Ponci, and A. Monti, "Analysis of a multi-timescale framework for the voltage control of active distribution grids," *Energies*, vol. 14, no. 7, p. 1965, Apr. 2021.
[18] P. D. Christofides, R. Scattolini, D. M. de la Peña, and J. Liu, "Distributed model predictive control: A tutorial review and future research directions," *Comput. Chem. Eng.*, vol. 51, pp. 21–41, Apr. 2013.
[19] P. Trodden and A. Richards, "Cooperative distributed MPC of linear systems with coupled constraints," *Automatica*, vol. 49, no. 2, pp. 479–487, Feb. 2013.
[20] A. Simonetto and H. Jamali-Rad, "Primal recovery from consensus-based dual decomposition for distributed convex optimization," *J. Optim. Theory Appl.*, vol. 168, no. 1, pp. 172–197, Jan. 2016.
[21] A. Falsone and M. Prandini, "A distributed dual proximal minimization algorithm for constraint-coupled optimization problems," *IEEE Control Syst. Lett.*, vol. 5, no. 1, pp. 259–264, Jan. 2021.
[22] I. Notarnicola and G. Notarstefano, "Constraint-coupled distributed optimization: A relaxation and duality approach," *IEEE Trans. Control Netw. Syst.*, vol. 7, no. 1, pp. 483–492, Mar. 2020.
[23] H. Zhu and H. J. Liu, "Fast local voltage control under limited reactive power: Optimality and stability analysis," *IEEE Trans. Power Syst.*, vol. 31, no. 5, pp. 3794–3803, Sep. 2016.
[24] A. Hauswirth, A. Zanardi, S. Bolognani, F. Dörfler, and G. Hug, "Online optimization in closed loop on the power flow manifold," in *Proc. IEEE Manchester PowerTech*, Jun. 2017, pp. 1–6.
[25] A. Bernstein and E. Dall'Anese, "Real-time feedback-based optimization of distribution grids: A unified approach," *IEEE Trans. Control Netw. Syst.*, vol. 6, no. 3, pp. 1197–1209, Sep. 2019.
[26] M. Farivar, L. Chen, and S. Low, "Equilibrium and dynamics of local voltage control in distribution systems," in *Proc. 52nd IEEE Conf. Decis. Control*, Dec. 2013, pp. 4329–4334.
[27] S. Bolognani and S. Zampieri, "On the existence and linear approximation of the power flow solution in power distribution networks," *IEEE Trans. Power Syst.*, vol. 31, no. 1, pp. 163–172, Jan. 2016.
[28] E. De Din, M. Pau, F. Ponci, and A. Monti, "A coordinated voltage control for overvoltage mitigation in LV distribution grids," *Energies*, vol. 13, no. 8, p. 2007, Apr. 2020.
[29] A. Camisa, F. Farina, I. Notarnicola, and G. Notarstefano, "Distributed constraint-coupled optimization via primal decomposition over random time-varying graphs," *Automatica*, vol. 131, Sep. 2021, Art. no. 109739.
[30] D. P. Bertsekas, *Nonlinear Programming*. Belmont, MA, USA: Athena Scientific, 1999.
[31] B. Stellato, G. Banjac, P. Goulart, A. Bemporad, and S. Boyd, "OSQP: An operator splitting solver for quadratic programs," *Math. Program. Comput.*, vol. 12, no. 4, pp. 637–672, Dec. 2020.
[32] *PYPOWER*. Accessed: Sep. 22, 2021. [Online]. Available: https://pypi.org/project/PYPOWER
[33] *Flexible Smart Metering for Multiple Energy Vectors With Active Prosumers*. Accessed: Mar. 21, 2022. [Online]. Available: https://ec.europa.eu/inea/en/horizon-2020/projects/h2020-energy/grids/flexmeter
[34] M. Pau, A. Angioni, F. Ponci, and A. Monti, "A tool for the generation of realistic PV profiles for distribution grid simulations," in *Proc. Int. Conf. Clean Electr. Power (ICCEP)*, Jul. 2019, pp. 193–198.

EDOARDO DE DIN received the M.S. degree *(cum laude)* in electrical engineering from the University of Trieste, Trieste, Italy, in 2015. He is currently with the E.ON Energy Research Center, Institute for Automation of Complex Power Systems, RWTH Aachen University, Aachen, Germany, where he is currently pursuing the Ph.D. degree. His current research interests include design of voltage control algorithms for distribution systems and the development of distribution grid automation services.

MARTINA JOSEVSKI received the Ph.D. degree in mechanical engineering from RWTH Aachen University, Aachen, Germany, in 2018. From 2018 to 2021, she was a Postdoctoral Research Associate with the E.ON Energy Research Center, Institute for Automation of Complex Power Systems, RWTH Aachen University, where she was leading the team for advanced control methods in power system applications. She is currently a Lead Research Engineer and a Project Manager at Eaton Research Labs, Eaton Corporation, where she is coordinating research activities related to novel power conversion technologies and supporting digital services. She is also active as an External Lecturer at RWTH Aachen University. Her current research interests include modeling of DC and hybrid power systems, optimal control of low-inertia power systems, and distributed optimization with specific focus to model predictive control.

MARCO PAU (Member, IEEE) received the M.S. degree *(cum laude)* in electrical engineering and the Ph.D. degree in electronic engineering and computer science from the University of Cagliari, Italy, in 2011 and 2015, respectively. He is currently a Senior Researcher at the Fraunhofer Institute for Energy Economics and Energy System Technology, where he works at the unit of grid planning and operation. His main research interests include monitoring and control of distribution grids and the design of solutions for distribution grid automation.

FERDINANDA PONCI (Senior Member, IEEE) received the Ph.D. degree in electrical engineering from the Politecnico di Milano, Italy, in 2002. She has been with the Department of Electrical Engineering, University of South Carolina, Columbia, SC, USA, as an Assistant Professor, since 2003. Since 2009, she has been with the E.ON Research Center, Institute for Automation of Complex Power Systems, RWTH Aachen University, Aachen, Germany, where she is currently a Professor of monitoring and distributed control for power systems.

ANTONELLO MONTI (Senior Member, IEEE) received the M.Sc. degree *(summa cum laude)* and the Ph.D. degree in electrical engineering from the Politecnico di Milano, Italy, in 1989 and 1994, respectively. He started his career at Ansaldo Industria. In 1995, he move to the Politecnico di Milano as an Assistant Professor. In 2000, he joined the Department of Electrical Engineering, University of South Carolina, Columbia, SC, USA, as an Associate Professor, and then a Full Professor. Since 2008, he has been the Director of the E.ON Energy Research Center, Institute for Automation of Complex Power System, RWTH Aachen University. Since 2019, he holds a double appointment with Fraunhofer FIT, where he is developing the new Center for Digital Energy, Aachen. He is the author or coauthor of more than 400 peer-reviewed papers published in international journals and proceedings of international conferences. He was a recipient of the 2017 IEEE Innovation in Societal Infrastructure Award. He is an Associate Editor of *IEEE Electrification Magazine*, a member of the Editorial Board of the *Sustainable Energy, Grids and Networks* (SEGAN) journal (Elsevier), and a member of the Founding Board of the *Energy Informatics* journal (Springer).